PAPER REF:

NUMERICAL AND EXPERIMENTAL CHARACTERIZATION OF STEEL–WOOD DOWELED JOINTS UNDER QUASI-STATIC LOADING

Nuno Dourado[1(*)], Marcelo de Moura[2], Abílio de Jesus[2], José Xavier[1,3]

[1] CITAB/UTAD, Departamento de Engenharias, Quinta de Prados, 5001-801 Vila Real, Portugal
[2] Institute of Mechanical Engineering (IDMEC), University of Porto, Porto, Portugal
[3] INEGI / LOME / LABIOMEP Campus da FEUP Rua Dr. Roberto Frias, 400 4200-465 Porto
[(*)] *Email*: nunodou@gmail.com

ABSTRACT

This objective of this work is to investigate the quasi-static mechanical behaviour of dowel-type timber joints. Therefore, four dowel arrangements were experimentally tested to assure the stability of a steel-wood joint. The results revealed different behaviour regarding the distance between dowels and distance to the free edge of the wood member. An approach based on cohesive zone modelling was adopted to replicate both the ductile and brittle failure observed in the experiments.

Keywords: Wood, dowel-joints, cohesive zone modelling.

INTRODUCTION

It is recognized that the resistance and durability of timber structures is largely dependent of the design of joints, which are clearly the weakest points in structures of this type. The loss of perfect continuity in timber structures caused by the presence of joints, leads to the reduction of global strength. Also, the highly orthotropic nature of wood causes dissimilar tension and compression behaviour in wood members. Dowel-type connections are the most common technique used to assure the fastening of timber elements. These technical solutions have been designed on the basis of the analytical Johansen's model (Johansen, 1949), being the modus operandi preconized in Civil Engineering codes like Eurocode 5 (CEN, 2004). The Johansen's model however only predicts ductile failure loads (crushing of wood and plastic bending of the dowel). The brittle failure observed both in single and multi-fastener arrangements (e.g., block shear, plug shear and cracking normal to grain) are not previewed by this model. Consequently, this limitation constitutes a major drawback, as brittle failure is responsible for catastrophic collapses in these structures. To prevent these failure modes, code procedures recommend minimum distances between fasteners as well as member side distances (CEN, 2004).

It is thus recognized that the development of advanced numerical models based on phenomenological aspects of wood failure are needed to simulate with accuracy the whole load-displacement curves of doweled joints. Being so, these models ought to replicate with accurateness both the brittle and ductile nature characteristic of wood. These models have also to account for local contact stresses between fasteners and wood members, interaction effects between multiple fasteners, the three-dimensional nature of the problem, among other parameters (Caldeira, 2014).

EXPERIMENTS

Fig. 1 shows the experimental arrangement formed by two wood members (*Pinus pinaster* Ait.) and a steel panel dully fastened to four steel dowels with diameter D = 14 mm. Those arrangements were distinguished by the distance between the dowels along the grain direction (L_1) and the distance to the member edge (L_2). The used distances were defined as multiples of D forming a total of four series: 4*D*-3*D*, 4*D*-4*D*, 5*D*-3*D* and 5*D*-4*D* (i.e., 3*D* = 42 mm; 4*D* = 56 mm and 5*D* = 70 mm).

The displacement rate was set to 0.5 mm as to avoid the activation of viscoelastic mechanisms of wood. Following an elastic response a non-linear behavior was observed in the load-displacement curves, which is characteristic of quasi-brittle materials like wood. The accurate analysis of the holes revealed the absence of plastic deformation in both metallic dowels and wood, which proves that the applied energy was only dissipated in damage mechanisms of wood. These mechanisms are due to the fibrous nature of wood that lead to the formation of micro-cracks and fiber-bridging in the wake of the formed cracks. These cracks were only visible in the vicinity of the dowels with important extents (Fig. 2). The attainment of the ultimate load was followed by sudden load drops (Fig. 3), which are more visible in those series that show higher values of edge distances (i.e., second indexes: from 3*D* to 4*D*). This observation was valid for both tested dowel distances (i.e., first indexes: from 4*D* to 5*D*).

Table 1 resumes the set of mean values of initial stiffness and ultimate load obtained in the experiments using 3 specimens per series. These results reveal that the reduction in the dowels distance (i.e., first index: 5*D* to 4*D*) for the same edge distance (i.e., second index: 3*D* or 4*D*) led to a reduction of the initial stiffness. The observed reduction was equal to 24.3% using an edge distance of 3*D* and 12.3% for 4*D*. This comparison is possible to execute since the stiffness differences are not negligible (higher than 10%) and the values of CoV are the relatively low (i.e., smaller or equal to 20%). It was observed a reduction in the initial stiffness with the increase of the beam free edge distance (i.e., second index: 3*D* to 4*D*). This reduction was equal to 29.8% for the dowels distance equal to 5*D*, and 18.6% for a distance between dowels equal to 4*D* (i.e., first index). Once again, this comparison is statistically possible to accomplish since the differences between stiffness are sufficiently important (i.e., higher than 18.6%) and the scatter is small (lower or equal to 20%).

The reduction in the dowels distance for the same edge distance (i.e., first index: 3*D* or 4*D*) has revealed that the ultimate load is statistically equal for series 5*D*-3*D* vs. 4*D*-3*D* and 5*D*-4*D* vs. 4*D*-4*D*. However, it is clear that the increase in the edge distance (i.e., second index: from 3*D* to 4*D*) has led to a decrease in the load bearing capacity of 32.5% (on average).

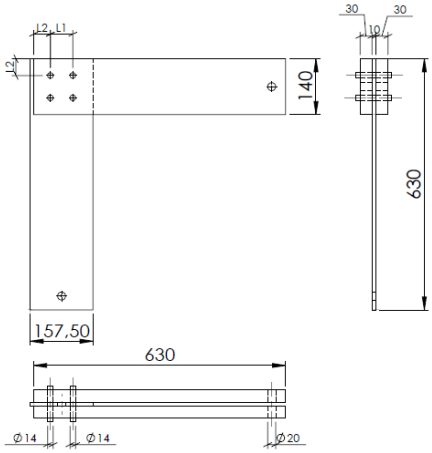

Fig. 1 – Structural arrangement.

Fig. 2 – Experimental setup.

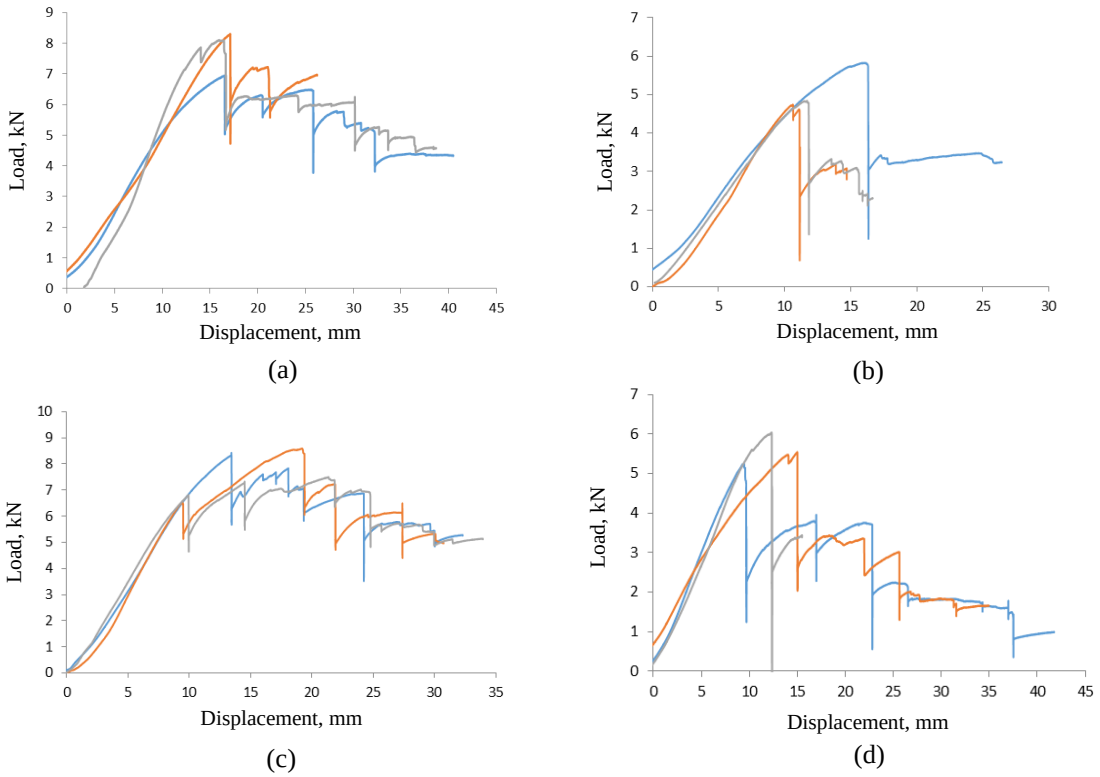

Fig. 3 – Experimental *P*-δ curves obtained for series: (a) 4*D*-3*D*, (b) 4*D*-4*D*, (c) 5*D*-3*D* and (d) 5*D*-4*D*.

Table 1 - Resume of the results obtained in the experiments.

Series	Stiffness (N/mm)		Ultimate load (kN)	
	Avg	CoV	Avg	CoV
4*D*-3*D*	601.6	20.0%	7.784	7.7%
4*D*-4*D*	489.6	7.0%	5.138	9.5%
5*D*-3*D*	795.1	6.1%	8.171	5.8%
5*D*-4*D*	558.2	4.2%	5.639	7.1%

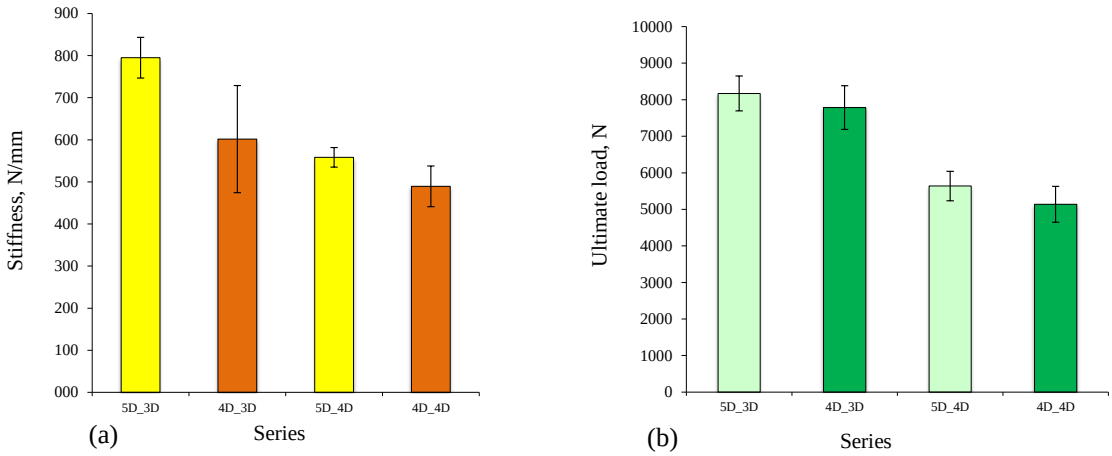

Fig. 4 – Initial stiffness (a) and ultimate load (b) obtained in the experiments.

NUMERICAL ANALYSIS

Damage initiation and propagation in wood has been simulated using a cohesive mixed-mode I+II model, using the linear softening relationship between stress and relative displacements (Fig. 5). Under pure mode loading the local strength $\sigma_{u,i}$ (i=I, II, III) and fracture toughness G_{ic} (area circumscribed by the triangle identified for pure-mode model I, II and/or III) are parameters that must be introduced. Thus, for pure mode loading (I, II or III) damage occurs when $\sigma_{u,i}$ is attained (for relative displacement $w_{o,i}$), growing as a function of a damage parameter, defined for the relative displacement w_i (Durão, 2006). Therefore, the total failure at a particular integration point is reached once the relative displacement attains $w_{u,i}$, which is determined by equating the value of the triangular area to G_{ic}.

Structures are usually submitted to mixed-mode loading, which means that the accurate simulation of its mechanical behaviour has to account for these complex loading cases. As a consequence, using the quadratic stress criterion to identify the damage initiation, turns

$$\begin{aligned} &\left(\frac{\sigma_{\mathrm{I}}}{\sigma_{\mathrm{u,I}}}\right)^2+\left(\frac{\sigma_{\mathrm{II}}}{\sigma_{\mathrm{u,II}}}\right)^2+\left(\frac{\sigma_{\mathrm{III}}}{\sigma_{\mathrm{u,III}}}\right)^2=1 \quad \text{if} \quad \sigma_{\mathrm{I}}\geq 0 \\ &\left(\frac{\sigma_{\mathrm{II}}}{\sigma_{\mathrm{u,II}}}\right)^2+\left(\frac{\sigma_{\mathrm{III}}}{\sigma_{\mathrm{u,III}}}\right)^2=1 \quad \text{if} \quad \sigma_{\mathrm{I}}\leq 0 \end{aligned} \tag{1}$$

considering that normal compressive stresses do not lead to damage initiation or propagation (Durão, 2006). Concerning damage propagation a linear fracture energetic criterion has been used (Durão, 2006),

$$\frac{G_{\mathrm{I}}}{G_{\mathrm{Ic}}}+\frac{G_{\mathrm{II}}}{G_{\mathrm{IIc}}}+\frac{G_{\mathrm{III}}}{G_{\mathrm{IIIc}}}=1 \tag{2}$$

By considering the relationship between stress and relative displacements ($\sigma_i = k_i w_i$, where k_i represents the interfacial stiffness), as well as between energies and stresses and relative displacements ($G_i = \sigma_i w_i/2$), both criteria (Eqs. (1) and (2)) can be established as a function of the squared values of equivalent relative displacement (i.e., w_m^2). The area circumscribed by the smaller triangle in Fig. 5 represents the energy contribution of each failure mode to the mixed-mode loading. Fig. 5 represents the maximum stress ($\sigma_{um,i}$) and critical value of the relative displacements ($w_{um,i}$). Hence, mixed-mode failure occurs when the dissipated energies in each mode (i.e., G_{I}, G_{II} and G_{III}) satisfy Eq. (2).

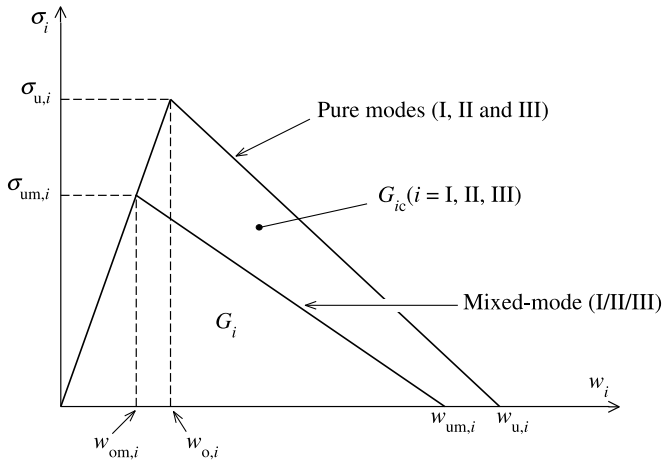

Fig. 5 - Pure (I, II or III) and mixed-mode (I/II/III) linear damage model.

The simulation of realistic stress distributions and corresponding influence on damage initiation and propagation in wood has been executed by means of a performed three-dimensional numerical analysis. The developed numerical model used approximately 34400 (8-node) (depending on the structural arrangement: Fig. 1) brick elements and 4400 (approx.) interface elements with zero-thickness (Durão, 2006). Attending to the symmetry of the experimental arrangement only an-half specimen was modeled (Fig. 6). Interface finite elements considering the mixed-mode (I/II/III) damage model permitted simulating the damage onset and propagation. These finite elements were disposed in successive layers along the grain direction of wood in the vicinity of the wood holes. In this model loading was imposed by prescribing the displacement value to the upper extreme dowel (Fig. 1) allowing the rotation of the lowest one. Non-linear analysis considering very tiny load increments (0.5% of the total applied displacement) was considered to guarantee smooth onset and propagation of damage in wood. Contact conditions were considered in the interfaces: wood-metal dowels and steel plate-wood member.

Tables 2 and 3 resume the elastic properties and fracture parameters of *Pinus pinaster* Ait. used in the numerical simulations. Fracture properties in mode III were assumed equal to those used in mode II. Dowels and metal plates were simulated as isotropic materials considering E = 210 GPa and ν = 0.35.

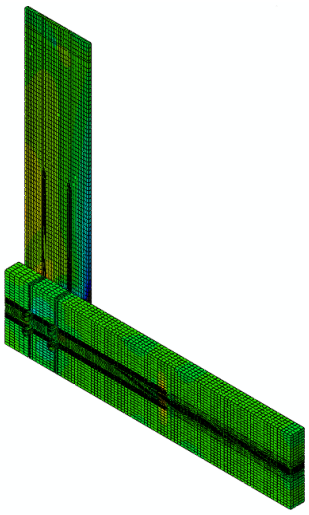

Fig. 6 – Three-dimensional finite element model.

Table 2 - Elastic properties of *Pinus pinaster* Ait. (Xavier, 2004; de Moura, 2009; Dourado, 2010)

E_L (GPa)	E_R (GPa)	E_T (GPa)	ν_{RT}	ν_{RL}	ν_{TL}	G_{RT} (GPa)	G_{RL} (GPa)	G_{LT} (GPa)
12.0	1.91	1.1	0.59	0.06	0.04	0.286	1.04	1.042

Table 3 - Cohesive parameters of *Pinus pinaster* Ait. for the RL fracture system (de Moura, 2009; Dourado, 2010, 2012)

G_{Ic} (N/mm)	G_{IIc} (N/mm)	$\sigma_{u,I}$ (MPa)	$\sigma_{u,II}$ (MPa)
0.26	0.91	5.34	9.27

NUMERICAL RESULTS

Figure 7 shows a detail of the developed numerical model in the vicinity of the dowels for series 4*D*-4*D*. The model has captured with remarkable accuracy the failure modes observed in the course of the loading process. Figure 8 permits observing the distribution of stresses (von Mises) that occurs along the dowel, as a consequence of bending, being coherent with the applied moment. Another noteworthy aspect as to do with the attained agreement of load-displacement curves (Fig. 9), using the formulation presented in the previous Section.

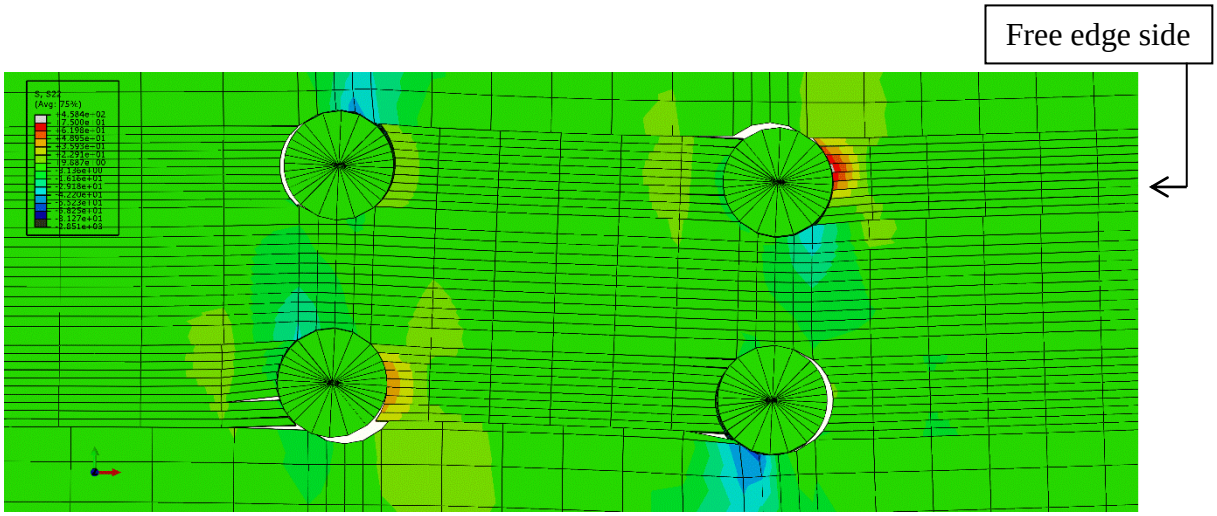

Fig. 7 – Stress field normal to grain in the vicinity of the dowels for series 4*D*-4*D*.

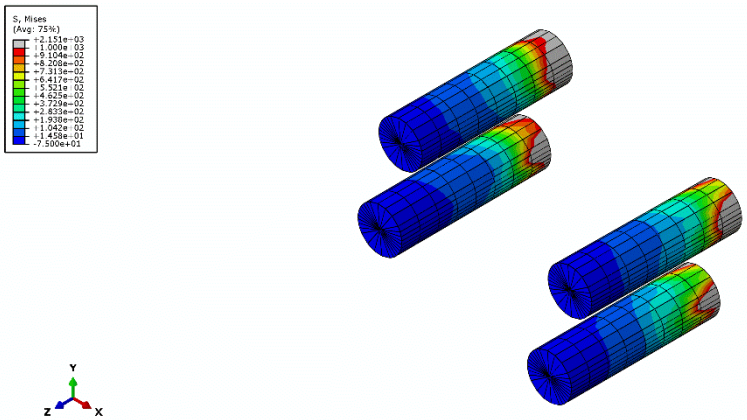

Fig. 8 – Stress field in the dowels.

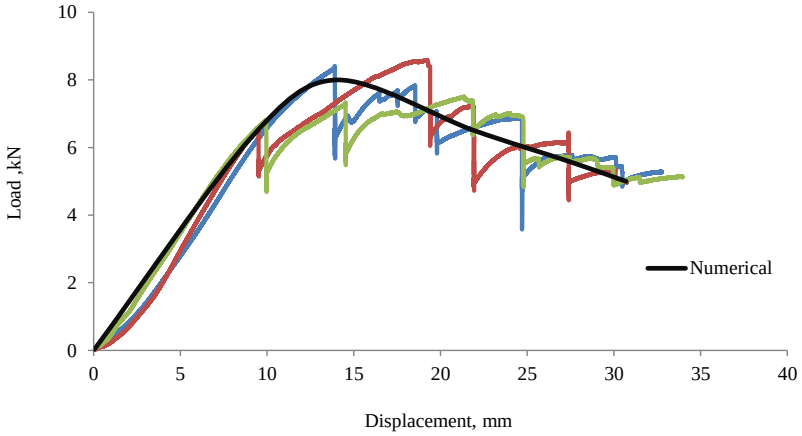

Fig. 9 – Agreement of load-displacement curves for series 4*D*-4*D*.

CONCLUSIONS

An investigation of the quasi-static mechanical behavior of dowel-type timber joints has been performed in the present work. Hence, four arrangements of dowels were experimentally analyzed, involving two distances between dowels and two distances to the wood free edge (multiples of the used dowel diameter *D*). The experiments revealed clear differences between those tested dispositions, both in the initial stiffness and load bearing capacity, with dissimilar scenarios in terms of loading drops in the post peak regime. In particular, it has been noticed a decrease in the initial stiffness when the distance between dowels was reduced, keeping the edge distance constant. A decrease of stiffness was also noticed with the increase of the free edge distance, for the same distance between dowels. On the other hand, non-remarkable differences have been observed in the load bearing capacity of the tested arrangements, with the reduction of the dowels distance, keeping the edge distance unchanged. However, a decrease in the load bearing capacity was perceived with the increase of the free edge distance.

An approach based cohesive zone modelling was adopted to replicate both the ductile and brittle failure observed in the experiments. A three-dimensional finite element model was developed, to mimic the mixed-mode (I+II) loading conditions. A fine agreement with the experimental load-displacement responses and developed cracks in the vicinity of the dowels have been achieved. As a consequence, one can affirm that the developed cohesive zone model was found apt to predict with accuracy the mechanical behavior of the tested arrangements.

ACKNOWLEDGEMENTS

The second author acknowledges the “Comissão de Coordenação e Desenvolvimento Regional do Norte (CCDRN)” for the financial support by the Operational Programme of the North Region (ON2) (Grant no. 07-0124-000033), under the research Project “Compo- site Materials, Structures & Processes, Operation, NORTE-07-0124-FEDER-000033”.

REFERENCES

Johansen KW. Theory of Timber Connections. International Association for Bridge and Structural Engineering. IABSE Journal, 1949, 9, p. 249-262.

CEN-TC250. EN 1995-1-1 Design of Timber Structures. Part 1-1: General Rules and

Rules for Buildings. European Standards, 2004, Brussels.

Caldeira T.V.P., Dourado N., de Jesus A.M.P., de Moura M.F.S.F., Morais J. (2014). Quasi-static behavior of moment-carrying steel-wood doweled joints. Construction & Building Materials. 53: 439–447.

Durão L.M., de Moura M.F.S.F., Marques A.T. (2006). Numerical Simulation of the Drilling Process on Composites, Compos Part A-Applied Science. 37:1325-1333.

Xavier J., Garrido N., Oliveira M., Morais J., Camanho P., Pierron F. (2004). A comparison of shear characterization of Pinus pinaster Ait. With the Iosipescu and off-axis shear test methods. Compos Part A- Applied Science. 35:827-840.

de Moura M.F.S.F., Silva M.A.L., Morais J.J.L., de Morais A.B., Lousada J.J.L. (2009). Data reduction scheme for measuring GIIc of wood in end-notched flexure (ENF) tests. Holzforschung. 63:99-106.

Dourado N., de Moura M.F.S.F., Morais J.J.L., Silva M.A.L. (2010). Estimate of resistance-curve in wood through the double cantilever beam test. Holzforschung. 64:119-126.

Dourado N., Pereira F.A.M., de Moura M.F.S.F., Morais J.J.L. (2012). Repairing wood beams under bending using carbon-epoxy composites. Engineering Structures. 34:342-50.